Journal of Biomechanics 82 (2019) 20–27

Contents lists available at ScienceDirect

Journal of Biomechanics

journal homepage: www.elsevier.com/locate/jbiomech
www.JBiomech.com

Towards optimal flow diverter porosity for the treatment of intracranial aneurysm

Yue Zhang [a,1], Yan Wang [b,*,1], Evan Kao [b], Leonardo Flórez-Valencia [c], Guy Courbebaisse [d]

[a] Department of Surgery, University of California, San Francisco, San Francisco, United States
[b] Department of Radiology, University of California, San Francisco, San Francisco, United States
[c] Pontificia Universidad Javeriana, Bogot, Colombia
[d] University of Lyon, INSA-Lyon, Universit Claude Bernard Lyon 1, UJM Saint-Etienne, CNRS, INSERM, CREATIS UMR 5220, U1206, F69621 Lyon, France

ARTICLE INFO

Article history:
Accepted 7 October 2018

Keywords:
Intracranial aneurysm
Patient-specific geometry
Fully-resolved flow diverter stent
Lattice Boltzmann method
Blood flow simulation
Wall shear stress
Thrombosis

ABSTRACT

Purpose: Low-porosity endovascular stents, known as flow diverters (FDs), have been proposed as an effective and minimally invasive treatment for sidewall intracranial aneurysms (IAs). Although it has been reported that the efficacy of a FD is substantially influenced by its porosity, clinical doctors would clearly prefer to do their interventions optimally based on refined quantitative data. This study focuses on the association between the porosity configurations and the FD efficacy, in order to provide practical data to help the clinical doctors optimize the interventions.
Method: Numerical simulations in fluid dynamics were performed using four patient-specific IA geometries, pulsatile velocity profiles and braided fully resolved FDs. The variation of velocity and wall shear stress within the IAs, were investigated in this study. Lattice Boltzmann method (LBM) was used to solve the main challenge centered on the diversity of spatial scales since the typical diameter of struts of FDs is only 25 μm while the artery normally can be larger by a hundred times.
Results: Numerical simulations revealed that the blood flow within IA sac was substantially reduced when the porosity is less than 86%. In particular, the flow condition within each IA sac is favorite to initialize thrombus formation when porosity is less than 70%.
Conclusion: Our study suggests the existence of a porosity threshold below which the efficacy of a FD will be sufficient for the patients to initialize the thrombus formation. Therefore, by estimating the porosity of FD on patient-specific information, it may be potentially to predict whether or the blood flow condition will successfully become prothrombotic after the FD intervention.

1. Introduction

An intracranial aneurysm (IA) is a vascular disorder characterized by a distension of the vessel wall that may rupture under certain circumstances. The rupture can lead subarachnoid hemorrhage which has been reported with high morbidity and mortality rates (Wiebers et al., 2003). The principal aim of endovascular treatment of IA is to reduce blood flow within the IA sac and redirect the bloodstream into the parent artery. A flow diverter (FD) has been reported as one of the current optimal minimally invasive treatments for IAs (Kallmes et al., 2007). Multiple clinical studies (Berge et al., 2012; Murthy et al., 2014) have been performed in order to demonstrate that FDs are able to slow down the IA blood flow, producing an inflammatory response followed by thrombosis, which can eventually, stabilize the IA and lead to an improvement in the patient health. In addition to biochemical factors, hemodynamics are thought to play a key role in understanding the IA growth, the consequent thrombus formation and the possible wall rupture. Many hemodynamic variables, including velocity and wall shear stress (WSS), are studied to understand these mechanisms (Steiger, 1990). For over a decade, hemodynamics has been studied using computational fluid dynamics (CFD) (Sforza et al., 2009) and many studies have demonstrated that CFD techniques can provide a detailed analysis on the flow in patient-specific cases (Wang et al., 2015; Zhang, 2015; Noël et al., 2017; Wang, 2014). Recently, it has also been shown that investigation on hemodynamics after FD insertion using CFD can be in good agreement with the *in vitro* experiments (Cito et al., 2015). Despite the success that has been made in treating IAs using FD devices, the permanent morbidity (10%) and mortality (5%) associated with the FDs are

* Corresponding author.
E-mail address: 612ywnag@gmail.com (Y. Wang).
[1] Drs. Yue Zhang and Yan Wang are co-first authors.

https://doi.org/10.1016/j.jbiomech.2018.10.002
0021-9290/

not negligible (Arrese et al., 2013; Lubicz et al., 2010). Factors that affect the function or efficacy of a FD remain unclear and a better understanding of them could help clinical doctors improve their intervention. Particularly, critical parameters such as porosity could help clinicians determine the ideal FD configuration for triggering thrombus formation. However, the main difficulties that exist in analyzing the FD efficacy are that (1) researchers can hardly modify one parameter but keep the other conditions (e.g. vessel geometry and inlet velocity) unchanged (Arrese et al., 2013); and (2) the cost will be considerably high to implement experiments using FDs with different configurations. To solve this issue, several studies took advantage of numerical simulations (Augsburger et al., 2009; Ma et al., 2014; Meng et al., 2006; Zhang et al., 2016). However, most simulation studies only reported employing artificial vascular geometries to simulate the complex FD-vessel system due to the lack of suitable stent-deployment technique, the FD porosity calculation method for patient-specific models, and the extremely high computational cost on the numerical simulations. Berg et al. reported hemodynamic simulations for two patient-specific models with single FD configuration (Berg et al., 2018); Li et al. presented their screen-based application using an 2D artificial aneurysm (Li et al., 2018); Suzuki et al. investigated the relationships between geometrical parameters and mechanical properties using 5 stents (Suzuki et al., 2017); Zhang et al. employed three vascular geometries to investigate the proposed optimization method under various hemodynamic conditions (Zhang et al., 2016). Although those studies suggested that FD efficacy in reducing blood flow within the IA sac may highly depend on its porosity, they also declared that more refined conclusions should be provided with the patient-specific geometries and the fully resolved FD model (Kim et al., 2010). Meanwhile, the experiments with FDs deployed into the abdominal aortas of rabbits revealed that it may be a high risk to deploy a FD with porosity less than 60% because of the existence of the intimal coverage of branch ostia (Hong et al., 2012). It's also noted that, based on observations from the THROMBUS project (http://www.thrombus-vph.eu), high-porosity FDs are easier to deploy and better for blood exchange between parent vessel and cavity. We hypothesize that a potential porosity threshold may exist, and this threshold can be used as a prediction for the success of a preventive endovascular treatment. The aim of this study is to conduct numerical simulations to estimate the potential porosity threshold. In order to realistically represent the reality in the medical surgery of FD deployment, the THROMBUS project recently developed a new technique to generate braided fully-resolved FDs interactively (Flórez-Valencia et al., 2012; Flórez-Valencia and Orkisz, 2017). This technique allows users to rebuild virtual FDs based on its commercial characteristics (e.g. the number of the struts and their weaving pattern) and takes the process of surgery into consideration by optimizing virtual deployment depending on the final length and configurations of the FDs used. It also can play with the deployment parameters in order to create virtual FDs with different porosity configurations. For example, if the user wants to create one FD with smaller porosity, he can simply increase the number of coils and/or the number of loops of each coil (note that in present study, we only modified the porosity by changing the number of loops of each coil since the number of coils of all FDs used in medical surgeries was 48). After generating FDs with different porosity configurations, the main challenges in this study center on the diversity of spatial scales (i.e. the diameter of artery is multiple orders of magnitude larger than that of the struts) and lengthy simulations. To cope with these issues, we run the blood simulations with the help of Lattice Boltzmann Method (Succi, 2001) (LBM) since it offers good calculation efficiency, simple boundary conditions, and reasonable accuracy, making it a powerful tool to deal with these issues. After this preliminary, we propose an adaptive framework to estimate the porosity of a FD deployed in patient-specific geometry. Additionally, we investigate the effect of the porosity configuration on FD efficacy based on patient-specific geometries and fully-resolved FDs.

2. Materials and methods

2.1. Patients' data and FD deployment

Four sidewall IAs shown in second row of Fig. 1 with different volumes ($984.3\ mm^3, 164.6\ mm^3, 55.0\ mm^3$ and $602.6\ mm^3$, respectively) were used in the present study. The position of IA (Shapiro et al., 2014) was taken into consideration: Patient 1 was located at a straight parent artery, Patient 3 was located at the inner curve of its parent artery while Patients 2 and 4 located at more outer of the vessel curve. These four patients geometries were reconstructed by THROMBUS project (Chen et al., 2014; Wang et al., 2016, 2017a). All patients were successfully treated with Pipeline Embolization Devices (Pipeline®) at the Radiology Department of the University Hospital Center in Montpellier, France. For each patient, the upstream velocity profile (shown in bottom row of Fig. 1) was acquired by clinical doctors using standard 2D phase-contrast magnetic resonance imaging and an in-house software application for segmenting medical images and estimating velocities (Eker et al., 2015). The virtual braided fully resolved FDs were interactively constructed in the vessel geometries of all the patients by our in-house application based on RGC-sm model (Flórez-Valencia et al., 2012; Flórez-Valencia and Orkisz, 2017). The start and end points for each virtual FD (see the middle row of Fig. 1) were determined with help of 2D digital subtracted angiography images (lateral, frontal and working views) acquired during the endovascular treatment as shown in the top row of Fig. 1. This technique produces collision-less struts, and also allows "weaving" the struts with different patterns. We used weaving patterns that matched the patterns of the actual FDs deployed in patients.

2.2. Porosity estimation using image segmentation methods

Porosity estimation on deployed FDs remains an open question, although a few methods have been reported (Augsburger et al., 2009; Larrabide et al., 2014). In this study, we proposed a precise and efficient framework (shown in Fig. 2 which can be simply read as, $Metal\ coverage = 100\% - Porosity$), which is defined as the ratio of the free neck area divided by the total neck area,

$$Porosity = \frac{A_N - A_{FD}}{A_N} \times 100\%, \tag{1}$$

where A_N and A_{FD} represent the total neck area (shown in Fig. 2c, rounded by the red curve) and area of the FD struts (shown in Fig. 2d, white lines in the red curve), respectively. First, we extracted the region of interest (the neck of the IA, shown in Fig. 2b) from the original image. The neck area is a diffuse region whose boundary is difficult to segment. We use the elliptically refined level set method (Wang et al., 2016) to segment the aneurysm neck (Fig. 2c), which is normally bounded by discontinuities and ellipse-like contours. We adopt the general expression for the elliptically segmentation energy formulation form

$$E = \alpha E_{level\ set} + \beta E_{ellipse} \tag{2}$$

where $E_{level\ set}$ represents the level set term and $E_{ellipse}$ embeds the ellipse-like shape prior. The weight α and β are the positive hyper-parameters that balance the influence of the two terms. When β is low, for example, in the extreme case $\alpha = 0$ and $\beta = 0$,

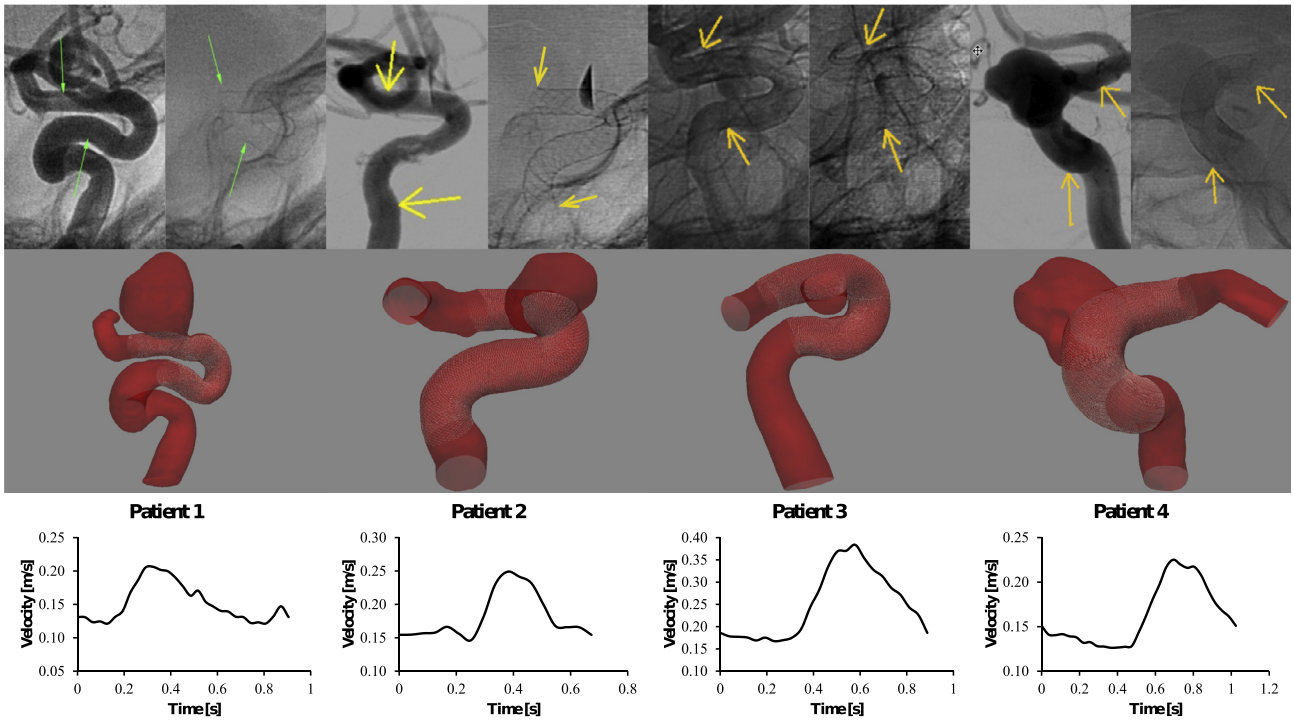

Fig. 1. The top row: 2D digital subtracted angiography images which were acquired during the treatment; the middle row: the start and end points for each virtual FD which were determined with help of 2D digital subtracted angiography images acquired during the endovascular treatment and a pattern of two up-one down of the struts was used for virtual deployment; the bottom row: patient-specific velocity profiles which were acquired by clinical doctors.

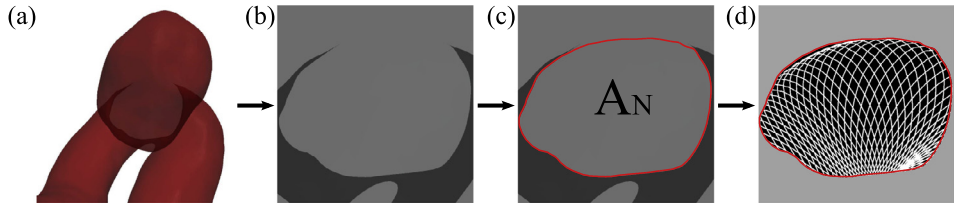

Fig. 2. Overview of the porosity estimation framework taking Patient 2 as an example. (a) the geometry of Patient 2, (b) neck extraction of Patient 2, (c) neck segmentation using level-set with ellipse method, (d) segmentation of struts of FD device using Otsu method.

this amounts to using the traditional level set segmentation; when β is high, the segmentation contour will be closer to an ellipse; in the extreme case $\beta = +\infty$, predominant weighting is given to the ellipsoid shape; for the intermediate β value ($\sim$1), local variations of the final contour are closer to those of actual contours. In all the experiments presented herein, α and β were set at 1 and 0.6, which has been observed to provide contours that follow the actual ones. The Chan-Vese model (Chan et al., 2000) is used in this present study as the level set term

$$\begin{aligned} E_{level\ set}(c_1, c_2, C) &= \mu \cdot Length(C) + v \cdot Area(inside(C)) \\ &+ w_1 \int_{inside(C)} |I - c_1|^2 dxdy + w_2 \int_{outside(C)} |I - c_2|^2 dxdy, \end{aligned} \tag{3}$$

where $\mu \geqslant 0, v \geqslant 0, w_1$ and $w_2 > 0$ are fixed parameters. I is intensity of the image, c_1 and c_2 are the average intensity inside and outside C, respectively. The annular shape constraint in our level set framework is developed by minimizing the following energy criterion:

$$E_{ellipse}(\phi, \lambda) = \int_{\Omega} (\phi(X) - \phi_e(X, \lambda))^2 \delta(\phi(X)) dX, \tag{4}$$

$$\phi_e(X, \lambda) = \frac{F(X, \lambda)}{|\nabla F(X, \lambda)|}, \tag{5}$$

$$F(X, \lambda) = \lambda_1 X^2 + \lambda_2 Xy + \lambda_3 y^2 + \lambda_4 X + \lambda_5 y + \lambda_6 \quad with\ \ \lambda_2 < 4\lambda_1\lambda_3, \tag{6}$$

where $\phi_e(X)$ is the Sampson distance function (Wang et al., 2016) representing the Sampson distance of a point X from the annular shape defined by the parameter λ. The function $F(X, \lambda)$ corresponds to the algebraic distance of a point $X = (x, y)$ to an ellipse and is represented by the standard quadratic equation for conic sections. The following equations are obtained based on the fact that we can obtain the minimization of energy by finding the geodesic zero level set:

$$\frac{\partial \phi}{\partial t} = g(X, \lambda)\delta(\phi(X)) \tag{7}$$

$$g(X, \lambda) = -2(\phi(X) - \phi_e(X, \lambda)). \tag{8}$$

After aneurysm neck is segmented, the Otsu method (Otsu, 1979) was performed to segment the struts (results shown in Fig. 2d). At last, with the segmentation results, the porosity can

be estimated through Eq. (1). The main objective of this study is to determine a porosity threshold that can help clinicians select the best device for triggering thrombus formation in their patients. In this stage, we included four patients and set up three different porosity levels (shown in Table 1), including the actual porosity level used in these patients (Level 3).

2.3. Segmentation parameter setting

The parameters α and β in Eq. (2) are the positive hyper-parameters that balance the influence of the level set and shape prior terms. As we discussed before, in all the experiments presented herein, α and β were set at 1 and 0.6, which has been observed to provide contours that follow the actual ones. The rest of the parameters used in level set segmentation were shown in Eq. (3), μ, v, w_1, and w_2 were determined based on the description in Chan et al. (2000). The level set iteration can slightly vary depending on the image. In our experiments, the calculation of each step was stopped when a convergence was reached ($\frac{A_N \cap A_{N-1}}{A_N} \times 100\% \leqslant 0.001$, where A_N represents the current segmentation result). During our experiments, the iteration for level set was basically around 300. All the parameters are summarized in Table 2.

2.4. Numerical simulations of blood flow with LBM

Blood flow simulations of IAs with FDs remain a challenge due to the range of spacial scales of the flow field. The typical diameter of the struts forming the FDs is as small as 25 μm, while the artery (3—5 mm) can be hundreds times larger. It is difficult to create a computational grid to adapt to these different spacial sizes, and the calculation of the fluid equations on such a grid can be even harder.

However, LBM (as described in similar studies (Succi, 2001)) offers the possibility to solve the fluid equations with a regular grid. Combining a so-called bounce-back boundary condition, we can simply identify all grid nodes located inside solid obstacles (like struts in the present study) and label them appropriately. LBM also allows us to fully resolve the flow pattern of blood flow on a grid with moderate resolution and at a reasonable computational expense, instead of using the analytical model to estimate the influence of the FDs.

Additionally, the THROMBUS project did a thorough convergence analysis to find an appropriate resolution for the numerical simulations. This analysis showed that the result would slightly depend on the resolution when the measurement points were chosen close to the FD. However, for measurement points far from the FD, grid convergence was reached if the grid spacing *dx* was within an order of magnitude of the strut diameter. This study concluded that, for the purpose of a velocity and WSS study in the IA, a grid resolution of the order of the strut diameter is sufficient (the grid spacing in this study was 29 μm). It also was found that for the present study, a dimensionless lattice velocity of $u_{LB} = 0.04$ can provide sufficient accuracy. For each patient, this approach was used to impose a no-slip boundary condition along the blood vessel wall, a Dirichlet boundary condition with a time-oscillating Poiseuille profile at the inlet, and constant-pressure boundary condition at the outlet (as described in similar studies (Succi, 2001)). Furthermore, considering that in larger vessels (diameter >0.5 mm) blood behaves as a Newtonian fluid (Nichols et al., 2011), an incompressible viscous Newtonian fluid with density $\rho = 1060\ \mathrm{kg/m^3}$ and kinematic viscosity $v = 3.3 \times 10^{-6}\ \mathrm{m^2/s}$ was assumed in this study. In order to reduce initial transients, two cardiac cycles were computed and data of the second was analyzed. All the simulations were performed with the open source library Palabos (http://www.palabos.org) based on LBM, which is a validated CFD tool for the study of flow dynamics (Malaspinas et al., 2016), and the parallel computations have been performed on the cluster of the CC-IN2P3- CNRS (http://cc.in2p3.fr).

Table 1
Different porosity levels for four patients to find the optimized porosity configuration.

	Level 0	Level 1	Level 2	Level 3
Patient 1	100	86	78	70
Patient 2	100	86	78	69
Patient 3	100	86	78	70
Patient 4	100	85	78	70

Table 2
Choice of segmentation parameters.

Parameters	α	β	*Iteration*	μ	v	w_1	w_2
Numbers	1	0.6	300	0.1	0	1	1

2.5. Lattice Boltzmann method

LBM has been successfully applied to the numerical simulation of flows, especially in complex geometries such as intracranial arteries (He et al., 2009) and interest in this method has grown rapidly in recent years (Malaspinas et al., 2007). One of its main advantages is that data communication between nodes is always local, which allows for efficient parallelization (Nourgaliev et al., 2003). LBM takes a mesoscopic approach from statistical physics. Basically, macroscopic properties, like pressures p and velocity $\boldsymbol{u}$ of a fluid, can be represented in terms of a discrete set of populations $f_i (i = 0, \ldots, k-1)$, which are discrete representation of the statistical particle distribution functions for the velocity of molecules. The total number of variables *k*allocated on every node of the lattice is model dependent, and reflects a choice of numerical stencil during the discretization of velocity space. The macroscopic density ρ and velocity $\boldsymbol{u}$ of fluid can be computed as moments of the populations,

$$\rho = \sum_i f_i \quad \boldsymbol{u} = \sum_i f_i \boldsymbol{e}_i, \tag{9}$$

where constant vector $\boldsymbol{e_i}$ represents the discrete velocity model in the discretization procedure of velocity space. The most widely known LBM model called lattice BGK (LBGK for short) was implemented in the present study (as described in similar studies (Succi, 2001)), in which the distribution functions f_i of each node relaxed on the same time-scale and towards a set of discrete equilibrium distribution functions f_i^{eq} parametrized by the local conserved quantities, density ρ and velocity $\boldsymbol{u}$. The LBM equation is exposed by,

$$f_i(\boldsymbol{x} + \Delta t \boldsymbol{e}_i, t + \Delta t) - f_i(\boldsymbol{x}, t) = -\frac{1}{\tau}[f_i(\boldsymbol{x}, t) - f_i^{eq}(\boldsymbol{x}, t)], \tag{10}$$

where τ is the relaxation time and f_i^{eq} are given by

$$f_i^{eq} = \omega_i \rho \left[1 + \frac{\boldsymbol{e}_i \cdot \boldsymbol{u}}{c_s^2} + \frac{(\boldsymbol{e}_i \cdot \boldsymbol{u})^2}{2c_s^4} - \frac{\boldsymbol{u} \cdot \boldsymbol{u}}{2c_s^2}\right], \tag{11}$$

where c_s is the sound speed of the lattice and w_i are the weight coefficients corresponding to the considered directions of the lattice. They both depend on the choice of lattice (see the coefficients selection (Succi, 2001)) and a three-dimensional (3D) lattice model called D3Q19 ($i = 0, \ldots, 18$) was used in this study. Meanwhile, the relaxation time τ in Eq. (10) is related to the kinematic viscosity v

through the relation, $\nu = c_s^2(\frac{\tau}{\Delta t} - \frac{1}{2})$ (Chen and Doolen, 1998; Malaspinas et al., 2007).

3. Results

3.1. Analysis of numerical simulations of four patients

Manual segmentation was used as the ground-truth for evaluating the automatic segmentation (Wang et al., 2016; Wang et al., 2017b), using the Dice value (Dice, 1945), a commonly used for measuring the overlap between manual and automatic segmentation. A MevisLab-based tool (http://www.mevislab.de/) was implemented to help our readers draw the manual contours. The manual IA neck segmentations of all subjects were performed in a blinded manner: one reader was blinded to the automated segmentation results. In this study, one reader drew manual contours two times in all subjects and the intra-observer variability was $1.54 \pm 1.30\%$. The contours obtained from the proposed automatic segmentation match well with the manual boundaries, with high Dice coefficients of $97.62 \pm 2.12\%$. This demonstrates that good and stable segmentation has been achieved with the proposed method on all subjects.

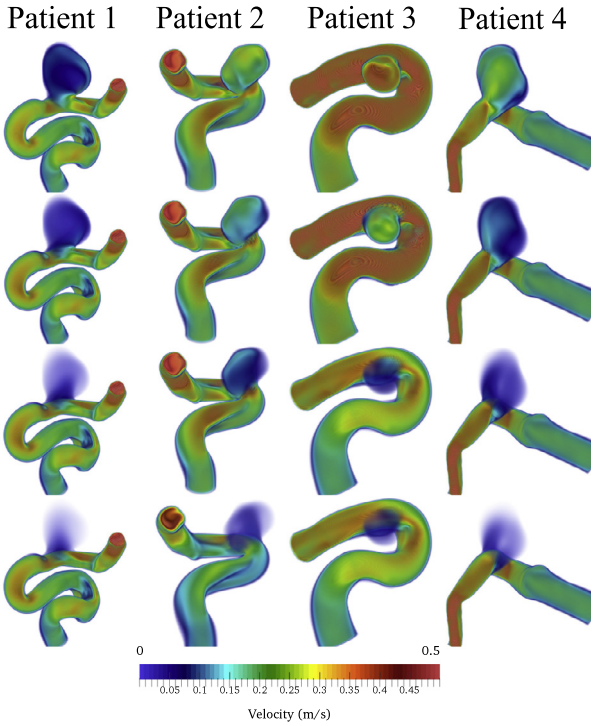

Fig. 3. The velocity magnitude distribution at peak systolic time in the pulsating flow condition for each IA. From top row to the bottom row: porosity configurations from level 0 to level 3. From left column to right: Patient 1 to Patient 4.

Before we started a general study on four patients, Patient 2 was chosen to conduct a preliminary test. We set up a relatively large range for porosity configuration, from 100% to 51.7%, (note that 100% means no FD deployed) for 10 cases, to find a correlation between the flow reduction and the porosity configuration. Our results for Patient 2 was similar to the trend proposed by Augsburger et al. (2009): the lower the porosity, the higher the flow reduction within the aneurysm sac.

After that, as we mentioned in Section 2.1, four groups of simulations were launched with different porosity levels (note that level 0 represents the cases without FD and level 3 corresponds to the FDs used in the medical intervention). Meanwhile, the patient-specific velocity profiles in treatment (shown in Fig. 1) were used as inlet velocity condition. The velocity distribution for each patient-specific model is shown in Fig. 3. It can be observed that for each case, the FD successfully disconnects the IA flow from the parent artery and restores a physiological flow. And for each case with FD, the velocity magnitudes within IA sac are reduced significantly while the behavior of blood flow within the parent artery remains almost the same as the case without FD. Furthermore, it also should be noted that for each case, the velocity magnitudes within IA sac stay considerably low for these four patients when the porosity is at Level 3.

Snapshots on velocity streamlines through the FDs are shown in Fig. 4, which were acquired at highest peak of the velocity profile. They reveals that the struts of FD devices block the blood flow and decrease its velocity. It can be noted that the velocities and the complexity of blood flow within the IA sac are substantially reduced after treatment. Furthermore, by decreasing the porosity, the flow structures may change and, in particular, become smoother and simpler (i.e. less swirling). The vortex size is reduced due to the placement of FD devices and the location of vortex center may shift from the dome to the center of the IA sac.

The variation of mean WSS of each IA sac surface during one cardiac cycle is provided in Fig. 5. A diversity of WSS reduction/reduction rate can be found, which will result in a great difficulty to predict FD efficacy for different patient-specific geometries. However, we note that the results clearly show that FDs reduce the WSS. For each patient-specific model, after the deployment of each FD, the peak of WSS almost occurs at same period of cardiac cycle. In other words, the WSS curve remains relatively similar shape as the case without FD. Another remark we would like to point out is that, for each IA model with a porosity of level 3, the mean WSS (even for the peak value) has been reduced considerably, which may lead to a favorite condition for initializing thrombus formation in patients, as observed.

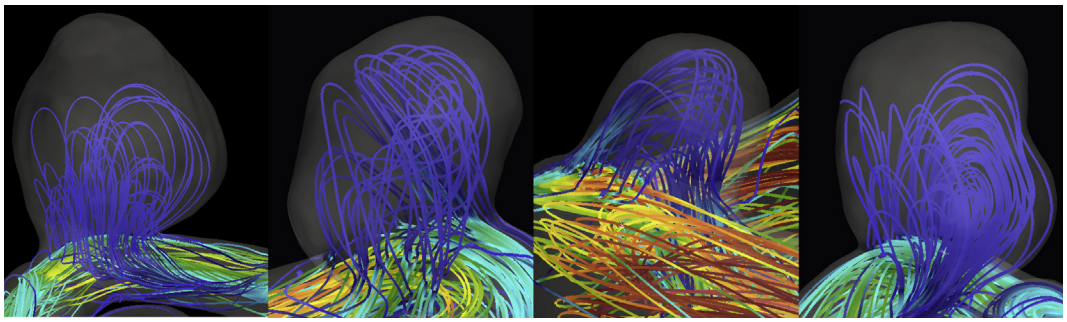

Fig. 4. The velocity streamlines distribution at peak systolic time in the pulsating flow condition for each IA. From left to right: from Patient 1 to Patient 4.

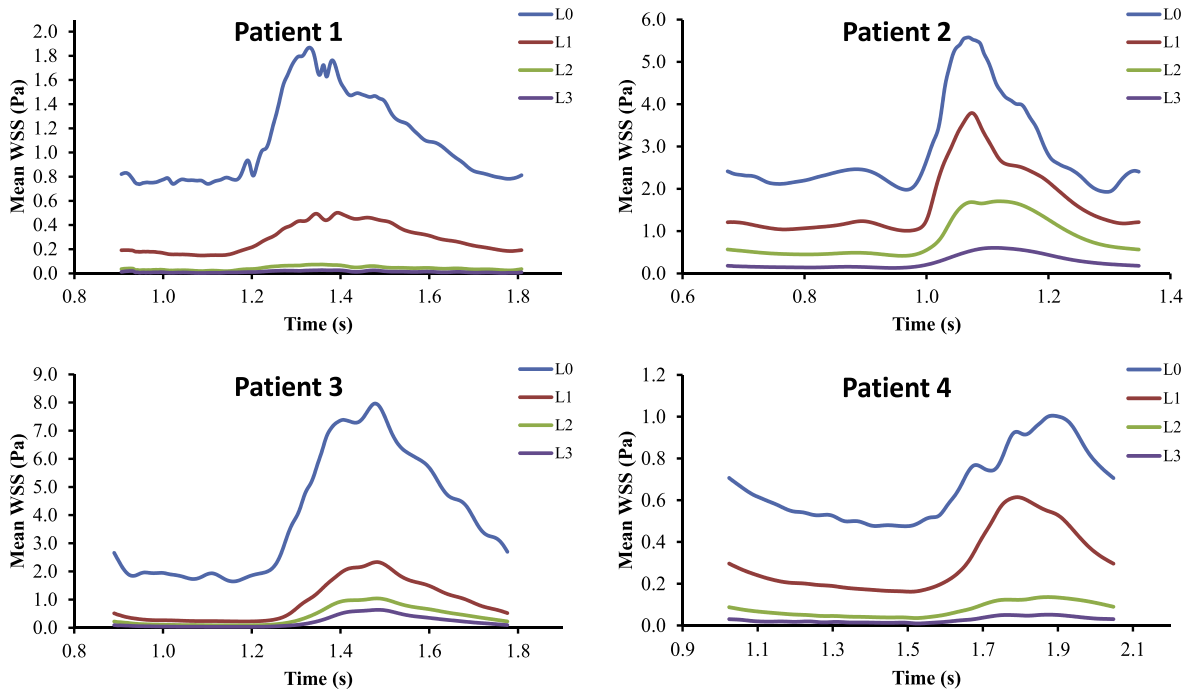

Fig. 5. The velocity magnitude distribution at peak systolic time in the pulsating flow condition for each IA. From top row to the bottom row: porosity configurations from level 0 to level 3. From left column to right: Patient 1 to Patient 4.

3.2. Quantitative analysis of the numerical simulations

In order to perform an in-depth study on the blood flow behavior, the WSS and the velocity within the IA sac, were evaluated. The average of mean velocity within the IA sac and mean WSS on the IA sac surface for each IA are analyzed and shown in Fig. 6. As we mentioned before, for each IA with the FD at same porosity level, a bigger reduction can be observed in WSS than in velocity. Meanwhile, a dropping reduction rate reveals a non-linear correlation between the porosity and the FD efficacy for each IA. Besides, one remark we would point out is that a variation in the reduction percentage can be observed for the four IAs (the quantitative data can be found in Table 3 and Fig. 6). For example, the velocity reduction reached 53.2% for the IA of Patient 3 with the porosity around 85% (level 1), while it is only 34.9% for the IA of Patient 2 under the same configuration. Also, the FD obtains lowest efficacy for the IA of Patient 1 when the porosity is around 85%, the FD makes highest efficacy when the porosity is around 65%. It reveals that, even with the porosity at the same level, the FD efficacy can vary largely depending on the patients. This fact suggests that, the volume size, the morphologic factors, and the inlet velocity of the IAs may also influence the FD efficacy. For example, if we take the volume of IAs mentioned in the beginning into consideration, the results shown in Fig. 6 indicate that, the FDs may have a better efficacy for the IAs with bigger volumes when the porosity is lower than 75%. In particular, the bigger the volume of IA is, the higher efficacy the FD may have.

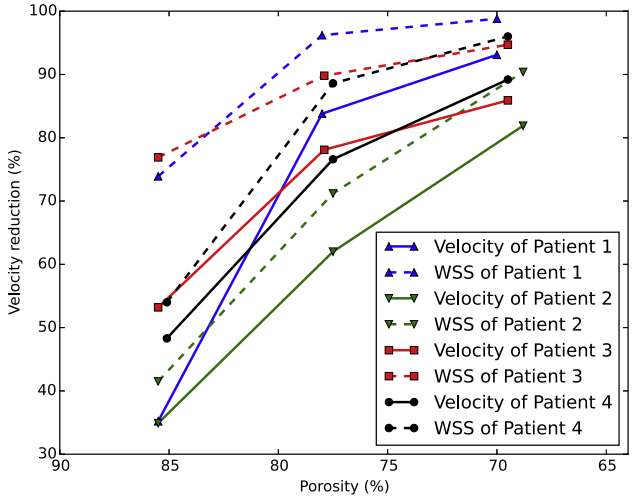

Fig. 6. The reduction percentage of the average of mean velocity within the IA sac and mean WSS on the IA sac surface for each IA with different porosity levels shown in Table 1.

Table 3
The average of mean velocity with IA sac (over one cardiac cycle) along with its reduction percentage for four patient-specific models with different porosity configurations.

	V_{sac} (m/s)			
	Patient 1	Patient 2	Patient 3	Patient 4
Level 0	0.078	0.166	0.230	0.098
Level 1	0.033	0.108	0.107	0.050
Level 2	0.013	0.063	0.050	0.023
Level 3	0.005	0.030	0.032	0.011

4. Discussion

Previous experiments with FDs deployed into the abdominal aortas of rabbits revealed that it may be a high risk to deploy a FD with porosity less than 60% because of the existence of the intimal coverage of branch ostia (Hong et al., 2012). We note that based on observations from THROMBUS project, high-porosity FD is easier to deploy and better for blood exchange between parent vessel and cavity. Although these findings show the clinical doctors and researchers a good path to follow, it still remains unclear to

predict the outcome of an intervention using a FD, due to the lack of more quantitative data.

The aim of this work is to provide a numerical study of virtual FDs to help in understanding the effect of porosity configurations on hemodynamics within the IAs and provide possible threshold for optimal porosity. To achieve this aim, patient-specific geometries and fully-realized FDs were used to establish numerical simulations. The virtual FDs were built based on their geometrical parameters from the manufacturers and their deployment location was validated by medical images.

In this study, the virtual insertion of the stent into the patient's vessels was proposed, which was subdivided into three steps: preprocessing, generation of stent geometrical characteristics, and virtual stent deployment. We have implemented a complete workflow to perform a virtual stent of intracranial aneurysms using pipeline flow diverters. Automatic level set based segmentation method was also proposed to estimate the porosity. The main difficulty in segmentation is contouring the aneurysm neck without the contour leakage. The proposed level set based segmentation method was developed to solve this problem by adding a shape prior term to the original level set formulation. The simulations have been carried out using lattice Boltzmann method.

According to our numerical simulations, there is no clear correlation between the porosity and FD efficacy for different IAs, which makes it extremely difficult to predict the FD efficacy with different porosity levels after the deployment. However, it should be noted that in the THROMBUS project, the clinical doctors successfully treated these patients with the FDs of level-3 porosity. Considering this fact and the finding that low velocity ($<$0.025 m/s) is normally associated with thrombus formation (Rayz et al., 2008; Malaspinas et al., 2016), our investigation on four patients indicates that a value of porosity around 70% can be sufficient for the patients to trigger the thrombus formation. Although it should be noted that there might exist different classes of IAs (i.e. different sizes or morphologies), for the most frequent ones, a potential universal porosity threshold may exist.

Despite the limitations of this study, our initial results suggest that the porosity equal to 65% would be a potential threshold which can be used as a prediction of the success of a preventive endovascular treatment using FD. The clinical doctors may take our study into consideration to make a patient-specific estimation of the FD efficacy before the intervention and to select the optimized device configuration for the patients.

5. Limitation and future directions

It should be noted that as the difference in diameter between the FD struts (25 μm) and the IA vessel is more than two orders of magnitude, it is very difficult to perform coupling calculation between the blood flow and the IA vessel wall or FD. This diameter difference also results in extremely high computational cost on simulations on the FD-vessel system. Small sample size has been a limitation in the simulation studies regarding this FD-vessel system. In the current work, 4 patient-specific models along with FD with different configurations were investigated. In future, more patients will be investigated to conduct a statistical analysis on the correlation between the FD efficacy and the porosity configuration and other FD brands will be considered as well to draw a more general conclusion.

6. Conclusions

In this article we investigated the effect of the FD porosity in the reduction of the blood flow within the IA being an important factor in the healing process, particularly the thrombus formation. Numerical simulations of one 3D patient-specific IA model of Patent 2 suggests that the efficacy of FDs is substantially associated with the porosity configuration. In particular, the efficacy will increase with decreasing porosity configurations (a non-linear correlation). Meanwhile, it was observed that the increased rate of efficacy of a FD slows down when we continue decreasing the porosity, especially when the porosity is lower than 70%. The numerical simulations of four patient-specific models show a variation in the FD efficacy with the porosity at same level. This observation suggests that morphologic factors, such as the volume and the relative location of IA, as well as the inlet velocity can partly influence the FD efficacy. The above facts make it hard to predict the FD efficacy with different porosity levels for different IAs. More patients would be needed to confirm the lack of correlation. Additionally, patient blood rheology, which affects the likelihood of clot formation, may also need to be taken into account by the simulation. However, considering the success made in the medical treatments for these patients, the present study indicates that a FD with a porosity around 70% will be sufficient for the treatment for the patients.

Conflict of Interest Statement

There is no conflict of interest.

Acknowledgment

The authors would like to express great appreciation to Dr. Bastien Chopard for his valuable and constructive advice during the planning and development of this research work and to Ricardo A. Corredor Jerez for his professional surpport in FD deployment technique.

This paper has been partly funded by the European Commission via the Thrombus project FP7-ICT-2009-6-269966 (http://www.thrombus-vph.eu).

References

Arrese, I., Sarabia, R., Pintado, R., Delgado-Rodriguez, M., 2013. Flow-diverter devices for intracranial aneurysms: systematic review and meta-analysis. Neurosurgery 73 (2), 193–200.

Augsburger, L., Farhat, M., Reymond, P., 2009. Effect of flow diverter porosity on intraaneurysmal blood flow. Clin. Neuroradiol. 19 (3), 204–214.

Berg, P., Saalfeld, S., Janiga, G., Brina, O., Cancelliere, N.M., Machi, P., Pereira, V.M., 2018. Virtual stenting of intracranial aneurysms: A pilot study for the prediction of treatment success based on hemodynamic simulations. Int. J. Artif. Organs. 0391398818775521.

Berge, J., Biondi, A., Machi, P., et al., 2012. Flow-diverter silk stent for the treatment of intracranial aneurysms: 1-year follow-up in a multicenter study. Am. J. Neuroradiol. 33 (6), 1150–1155.

Chan, T.F., Sandberg, B.Y., Vese, L.A., 2000. Active contours without edges for vector-valued images. J. Vis. Commun. Image Represent. 11 (2), 130–141.

Chen, S., Doolen, G.D., 1998. Lattice boltzmann method for fluid flows. Ann. Rev. Fluid Mech. 30 (1), 329–364.

Chen, Y., Navarro, L., Wang, Y., Courbebaisse, G., 2014. Segmentation of the thrombus of giant intracranial aneurysms from ct angiography scans with lattice boltzmann method. Med. Image Anal. 18 (1), 1–8.

Cito, S., Geers, A., Arroyo, M., 2015. Accuracy and reproducibility of patient-specific hemodynamic models of stented intracranial aneurysms: report on the virtual intracranial stenting challenge 2011. Ann. Biomed. Eng. 43 (1), 154–167.

Dice, L.R., 1945. Measures of the amount of ecologic association between species. Ecology 26 (3), 297–302.

Eker, O.F., Boudjeltia, K.Z., Jerez, R.A.C., 2015. Mr derived volumetric flow rate waveforms of internal carotid artery in patients treated for unruptured intracranial aneurysms by flow diversion technique. J. Cerebral Blood Flow Metabol. 35 (12), 2070–2079.

Flórez-Valencia, L., Orkisz, M., 2017. Right generalized cylinder model for vascular segmentation. In: Computing and Visualization for Intravascular Imaging and Computer-Assisted Stenting. Elsevier, pp. 131–156.

Flórez-Valencia, L., Serrano, E.D., Reyes, J.R., 2012. Virtual deployment of pipeline flow diverters in cerebral vessels with aneurysms to understand thrombosis. In: MICCAI-STENT'12 The 1st International MICCAI-Workshop on Computer Assisted Stenting. p. 49.

He, X., Duckwiler, G., Valentino, D.J., 2009. Lattice boltzmann simulation of cerebral artery hemodynamics. Comput. Fluids 38 (4), 789–796.
Hong, B., Wang, K., Huang, Q., 2012. Effects of metal coverage rate of flow diversion device on neointimal growth at side branch ostium and stented artery: an animal experiment in rabbit abdominal aorta. Neuroradiology 54 (8), 849–855.
Kallmes, D.F., Ding, Y.H., Dai, D., Kadirvel, R., Lewis, D.A., Cloft, H.J., 2007. A new endoluminal, flow-disrupting device for treatment of saccular aneurysms. Stroke 38 (8), 2346–2352.
Kim, Y.H., Xu, X., Lee, J.S., 2010. The effect of stent porosity and strut shape on saccular aneurysm and its numerical analysis with lattice boltzmann method. Ann. Biomed. Eng. 38 (7), 2274–2292.
Larrabide, I., Geers, A.J., Morales, H.G., Aguilar, M.L., Rüfenacht, D.A., 2014. Effect of aneurysm and ICA morphology on hemodynamics before and after flow diverter treatment. J. Neurointervent. Surgery, neurintsurg–2014.
Li, S., Latt, J., Chopard, B., 2018. The application of the screen-model based approach for stents in cerebral aneurysms. Comput. Fluids.
Lubicz, B., Collignon, L., Raphaeli, G., 2010. Flow-diverter stent for the endovascular treatment of intracranial aneurysms. Stroke 41 (10), 2247–2253.
Ma, J., You, Z., Byrne, J., Rizkallah, R.R., 2014. Design and mechanical properties of a novel cerebral flow diverter stent. Ann. Biomed. Eng. 42 (5), 960–970.
Malaspinas, O., Courbebaisse, G., Deville, M., 2007. Simulation of generalized newtonian fluids with the lattice boltzmann method. Int. J. Mod. Phys. C 18 (12), 1939–1949.
Malaspinas, O., Turjman, A., de Sousa, D.R., et al., 2016. A spatio-temporal model for spontaneous thrombus formation in cerebral aneurysms. J. Theoret. Biol. 394, 68–76.
Meng, H., Wang, Z., Kim, M., Ecker, R., Hopkins, L., 2006. Saccular aneurysms on straight and curved vessels are subject to different hemodynamics: implications of intravascular stenting. Am. J. Neuroradiol. 27 (9), 1861–1865.
Murthy, S.B., Shah, S., Rao, C.P.V., Bershad, E.M., Suarez, J.I., 2014. Treatment of unruptured intracranial aneurysms with the pipeline embolization device. J. Clin. Neurosci. 21 (1), 6–11.
Nichols, W., O'Rourke, M., Vlachopoulos, C., 2011. McDonald's Blood Flow in Arteries: Theoretical, Experimental and Clinical Principles. CRC Press.
Noël, R., Ge, F., Zhang, Y., Navarro, L., Courbebaisse, G., 2017. Lattice boltzmann method for modelling of biological phenomena. In: Signal Processing Conference (EUSIPCO), 2017 25th European. IEEE, pp. 2654–2658.
Nourgaliev, R.R., Dinh, T.-N., Theofanous, T.G., Joseph, D., 2003. The lattice boltzmann equation method: theoretical interpretation, numerics and implications. Int. J. Multiph. Flow 29 (1), 117–169.
Otsu, N., 1979. A threshold selection method from gray-level histograms. IEEE Trans. Syst., Man Cybernet. 9 (1), 62–66.
Rayz, V., Boussel, L., Lawton, M., 2008. Numerical modeling of the flow in intracranial aneurysms: prediction of regions prone to thrombus formation. Ann. Biomed. Eng. 36 (11), 1793.
Sforza, D.M., Putman, C.M., Cebral, J.R., 2009. Hemodynamics of cerebral aneurysms. Ann. Rev. Fluid Mech. 41, 91–107.
Shapiro, M., Raz, E., Becske, T., Nelson, P., 2014. Variable porosity of the pipeline embolization device in straight and curved vessels: a guide for optimal deployment strategy. Am. J. Neuroradiol. 35 (4), 727–733.
Steiger, H.-J., 1990. Pathophysiology of development and rupture of cerebral aneurysms. Acta Neurochir Suppl.
Succi, S., 2001. The lattice Boltzmann Equation: for Fluid Dynamics and Beyond. Oxford University Press.
Suzuki, T., Takao, H., Fujimura, S., Dahmani, C., Ishibashi, T., Mamori, H., Fukushima, N., Murayama, Y., Yamamoto, M., 2017. Relationships between geometrical parameters and mechanical properties for a helical braided flow diverter stent. Technol. Health Care 25 (4), 611–623.
Wang, Y., Zhang, Y., Navarro, L., et al., 2016. Multilevel segmentation of intracranial aneurysms in ct angiography images. Med. Phys. 43 (4), 1777–1786.
Wang, Y., Navarro, L., Zhang, Y., Kao, E., Zhu, Y., Courbebaisse, G., 2017a. Intracranial aneurysm phantom segmentation using a 4D lattice Boltzmann method. Comput. Sci. Eng. 19 (4), 56–67.
Wang, Y., Seguro, F., Kao, E., Zhang, Y., Faraji, F., Zhu, C., Haraldsson, H., Hope, M., Saloner, D., Liu, J., 2017b. Segmentation of lumen and outer wall of abdominal aortic aneurysms from 3d black-blood MRI with a registration based geodesic active contour model. Med. Image Anal. 40, 1–10.
Wang, Z., 2014. Analysis of carotid wall mechanics based on ultrasound imaging.
Wang, Z., Wood, N.B., Xu, X.Y., 2015. A viscoelastic fluid–structure interaction model for carotid arteries under pulsatile flow. Int. J. Num. Methods Biomed. Eng. 31 (5), e02709.
Wiebers, D.O., of Unruptured Intracranial Aneurysms Investigators, I.S., et al., 2003. Unruptured intracranial aneurysms: natural history, clinical outcome, and risks of surgical and endovascular treatment. The Lancet 362 (9378), 103–110.
Zhang, M., Anzai, H., Chopard, B., Ohta, M., 2016. Towards the patient-specific design of flow diverters made from helix-like wires: an optimization study. Biomed. Eng. Online 15 (2), 159.
Zhang, Y., 2015. Hemodynamic investigation and thrombosis modeling of intracranial aneurysms. Ph.D. thesis, INSA Lyon.